Λ hypernuclear production in $(K^-_{\rm stop}, \pi)$ reactions reexamined

V. Krejčiřík,[1,2,*] A. Cieplý,[2,†] and A. Gal[3,‡]
[1]*Faculty of Mathematics and Physics, Charles University, 12116 Prague, Czech Republic*
[2]*Nuclear Physics Institute, 25068 Řež, Czech Republic*
[3]*Racah Institute of Physics, The Hebrew University, 91904 Jerusalem, Israel*
(Received 13 May 2010; published 20 August 2010)

Distorted-wave impulse approximation calculations of Λ hypernuclear production rates in stopped K^- reactions on several p-shell targets used recently in experiments by the FINUDA Collaboration are reported. Chirally motivated $K^-N \to \pi\Lambda$ in-medium transition amplitudes are employed, and the sensitivity of the calculated rates to the initial K^--atomic wave functions and final pion distorted waves is studied. The calculated rates are compared with measured rates, wherever available, which confirm earlier observations that (i) the calculated rates are generally lower than the measured rates, and (ii) the deeper the K^--nuclear potential, the worse the discrepancy. The A dependence of the calculated $1s_\Lambda$ production rates is discussed, providing a useful tool to resolve the issue of depth of the K^--nuclear potential near threshold.

DOI: 10.1103/PhysRevC.82.024609 PACS number(s): 21.80.+a, 21.85.+d, 25.80.Nv, 36.10.Gv

I. INTRODUCTION

Λ hypernuclear production in $(K^-_{\rm stop},\pi)$ reactions, in which the final state is uniquely identified by measuring the outgoing pion momentum, was reported for the first time in stopped K^- experiments at CERN in 1973 [1] and more recently in experiments at KEK [2], BNL [3] and at DAΦNE, Frascati, by the FINUDA Collaboration [4–6]. On the theoretical side, several distorted-wave impulse approximation (DWIA) calculations of $(K^-_{\rm stop},\pi)$ hypernuclear production rates have been reported [7–11], but none of them led to satisfactory agreement with the measured rates.[1] In general, these calculated capture rates fall below the experimentally reported rates, with the exception of the old CERN data for ^{12}C [1].

The present paper primarily covers the production of $^{7}_{\Lambda}$Li, $^{9}_{\Lambda}$Be, $^{12}_{\Lambda}$C, $^{13}_{\Lambda}$C, and $^{16}_{\Lambda}$O, for all of which preliminary data have recently been reported [6]. We focus on the A dependence of the calculated rates, hitherto not explored systematically, to look for further tests of the role played by initial- and final-state interactions. In conjunction with previous calculations, we use the DWIA. Several K^--nuclear optical potentials are used to generate the required initial-state K^--atom wave functions (w.fs.), and several pion nuclear optical potentials are used to generate final-state pion distorted waves (DWs). The underlying $K^-N \to \pi\Lambda$ reaction amplitude is studied in free space, as well as in the nuclear medium, within the chiral Lagrangian framework [10,12–18] to generate in-medium branching ratios (BRs) for stopped K^- reactions. Past works [8–10] used BRs extrapolated from emulsion experiments [19]. We compare results obtained in both approaches.

The present paper is organized as follows. The capture at rest DWIA formalism is outlined in Sec. II. The choice of the microscopic chiral model for $K^-N \to \pi Y$ reactions at rest, together with the BRs derived in this model and the input w.fs. to the DWIA calculations, are specified in Sec. III. Results of Λ hypernuclear production rate calculations for stopped K^- reactions are presented and are discussed in Sec. IV, with a brief conclusion given in Sec. V.

II. CAPTURE AT REST CALCULATIONS

We study the reaction,

$$K^- + A(i) \longrightarrow \pi^{-\tau-1/2} + H(f), \tag{1}$$

in which a K^- meson is captured on a target nucleus denoted as A in its ground state i, from an atomic orbit nL into a final state f of a Λ hypernucleus H plus an outgoing pion. The superscript $-\tau - 1/2$ denotes the pion charge ($\tau = \pm 1/2$ for π^- and π^0, respectively). We follow the capture at rest calculation formalism detailed in Ref. [8]. In the DWIA, the nuclear reaction Eq. (1) is induced by the one-baryon transition,

$$K^- + N \longrightarrow \pi^{-\tau-1/2} + Y, \tag{2}$$

on a nucleon N to a hyperon Y, with the in-medium T matrix assumed here to be of the s-wave type:

$$T_{fi}(\mathbf{q}_f) = \sum_{j=1}^{\mathcal{N}} \langle f|t_j(\mathbf{q}_f)|i\rangle = t(q_f)\rho^{\rm DW}_{fi}(\mathbf{q}_f). \tag{3}$$

The charge indices are omitted for simplicity, and the DW transition form factor is given by

$$\rho^{\rm DW}_{fi}(\mathbf{q}_f) = \int d^3r\, \chi^{(-)*}_{\mathbf{q}_f}(\mathbf{r})\rho_{fi}(\mathbf{r})\Psi_{nLM}(\mathbf{r}), \tag{4}$$

where ρ_{fi} stands for the nuclear-to-hypernuclear transition matrix element. The K^--atomic w.f. Ψ_{nLM} is obtained by

*v.krejcirik@ujf.cas.cz
†cieply@ujf.cas.cz
‡avragal@vms.huji.ac.il
[1]Reference [11] is a preliminary conference version, which is outdated by the present paper.

solving the Klein-Gordon equation with a K^--nuclear strong interaction optical potential $V_{\rm opt}^K$ added to the Coulomb potential V_C generated by the nuclear charge distribution plus vacuum polarization. The dependence on the magnetic quantum number M was suppressed on the left-hand side of Eq. (4). The pion DW $\chi_{\mathbf{q}_f}^{(-)}$ in the final state is given in terms of a partial-wave expansion:

$$\chi_{\mathbf{q}_f}^{(-)*}(\mathbf{r}) = \sum_\ell (-\mathrm{i})^\ell (2\ell+1)\tilde{j}_\ell(r) P_\ell(\hat{\mathbf{q}}\cdot\hat{\mathbf{r}}). \tag{5}$$

The radial w.f. $\tilde{j}_\ell(r)$, which reduces to the spherical Bessel function $j_\ell(qr)$ for a free pion, solves the Klein-Gordon equation with the pion-nuclear optical potential plus the appropriate electromagnetic potential for a charged pion.

The nuclear capture rate per stopped K^- in the reaction Eq. (1) is given by

$$R_{fi}/K^- = \frac{q_f\omega_f}{\bar{q}_f\bar{\omega}_f} R(K^-N\to\pi\Lambda)\frac{\int d\Omega_{q_f}\left\langle\left|\rho_{fi}^{\rm DW}(\mathbf{q}_f)\right|^2\right\rangle}{4\pi\,\bar{\rho}_N}, \tag{6}$$

where the fractions $R(K^-N\to\pi\Lambda)$ are the elementary BRs for mononucleonic K^- absorption at rest in the nuclear medium. The brackets $\langle\cdots\rangle$ mean that the absolute square of the DW transition form factor is to be averaged on the initial states and summed over the final ones. The kinematical factor in front of R in Eq. (6) appears because of transformation of the two-body scattering amplitude, which describes the elementary reaction Eq. (2), into the many-body center-of-mass frame. The momentum q_f of the outgoing pion is determined by energy conservation, and ω_f stands for the reduced energy in the final state,

$$\begin{aligned} \omega_f^{-1} &= E_\pi^{-1}(q_f) + E_H^{-1}(q_f), \\ \omega_f &\longrightarrow E_\pi(q_f) \quad \text{for} \quad A\to\infty, \end{aligned} \tag{7}$$

where $\bar{q}_f$, $\bar{\omega}_f$ are appropriately averaged in-medium quantities. Finally, $\bar{\rho}_N$ denotes the effective nuclear density available to the K^- capture process,

$$\bar{\rho}_N = \int \rho_N(r)|R_{nL}(r)|^2 r^2\,dr, \tag{8}$$

where the nucleon density ρ_N and the K^--atomic radial w.f. are normalized according to

$$\int \rho_N\,d^3r = \mathcal{N}, \qquad \int |R_{nL}(r)|^2 r^2\,dr = 1, \tag{9}$$

where $\mathcal{N}$ denotes the number of neutrons or protons for $\tau = \pm 1/2$, respectively.

The last factor on the right-hand side of Eq. (6),

$$R_{fi}/Y = \frac{\int d\Omega_{q_f}\left\langle\left|\rho_{fi}^{\rm DW}(\mathbf{q}_f)\right|^2\right\rangle}{4\pi\,\bar{\rho}_N}, \tag{10}$$

is loosely termed the capture rate per hyperon Y because its derivation assumes that the capture reaction Eq. (2) is the only one available. It can be decomposed into contributions, which correspond to transitions with multipolarity k from a given n_Nl_N nuclear shell to a given n_Yl_Y hypernuclear shell, in the following form [8]:

$$R^k_{n_Nl_N\to n_Yl_Y} = \mathcal{N}(n_Nl_N)\frac{(2k+1)(l_N\,0\,k\,0\mid l_Y\,0)^2 N^k_{n_Yl_Y,n_Nl_N}}{4\pi\,\bar{\rho}_N}. \tag{11}$$

Here, $\mathcal{N}(n_Nl_N)$ is the neutron (proton) occupation number of the target nuclear shell for $\tau = +1/2(-1/2)$, the Clebsch-Gordan coefficient squared accounts for the conservation of angular momentum and parity, and the entities

$$N^k_{n_Yl_Y,n_Nl_N} = \sum_\ell (L\,0\,k\,0\mid\ell\,0)^2\left|I^\ell_{n_Yl_Y,n_Nl_N}\right|^2 \tag{12}$$

are the appropriate averages of the absolute squares of the DWIA amplitudes,

$$I^\ell_{n_Yl_Y,n_Nl_N} = \int_0^\infty dr\;\tilde{j}_\ell(r)u^*_{n_Yl_Y}(r)u_{n_Nl_N}(r)R_{nL}(r), \tag{13}$$

where $u_{n_Bl_B}(r)/r$ are the radial parts of the one-baryon w.fs. Equations (11)–(13) assume that the DWIA capture rate calculation does not depend on the total angular momenta $j_B = l_B \pm 1/2$ for the orbits in question. This was justified by the numerical calculation performed in Ref. [8], where more general formulas for the dependence on j_B can be found as well, and is checked later in the present paper.

III. INPUT

In this section, we specify the entities that are needed to perform numerical calculations of nuclear capture rates. First, we outline the model used for the one-baryon capture process Eq. (2). Subsequently, we specify the baryon and meson nuclear potentials chosen to generate initial- and final-state w.fs. for use in the evaluation of the DWIA amplitudes Eq. (13) that serve as input to nuclear capture rate calculations.

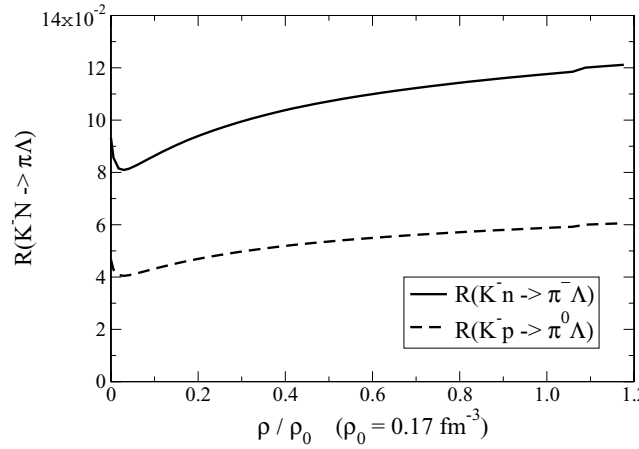

FIG. 1. Calculated BRs $R(K^-N\to\pi\Lambda)$ as a function of the nuclear density for capture on neutrons (solid curve) and on protons (dashed curve).

TABLE I. $R(K^-N \to \pi\Lambda)$ BRs (in units of 10^{-2}).

BR	BR1	BR2	BR3 [19]	
$R(K^-N \to \pi\Lambda)$	$\rho = \rho_0/2$	$\rho = 0$	^{12}C	^{16}O
$R(K^-n \to \pi^-\Lambda)$	10.54	9.68	8.7	7.7
$R(K^-p \to \pi^0\Lambda)$	5.27	4.84	4.4	3.9

A. $K^-N \to \pi\Lambda$ branching ratios

For the calculation of BRs $R(K^-N \to \pi\Lambda)$ of the one-baryon capture process Eq. (2), we adopted the effective potential model based on chiral symmetry, as described in detail in Refs. [12,13,16–18]. The required BRs are obtained in coupled-channel calculations that include ten meson-baryon channels coupled to the K^-p system [16,17]. We also take the effects of Pauli blocking and kaon self-energy in the nuclear medium into account [10,13,18]. The dependence of the calculated BRs on the nuclear density is demonstrated in Fig. 1 as a function of the fractional nuclear density ρ/ρ_0, where $\rho_0 = 0.17$ fm^{-3} is the nuclear-matter density. Although the central nuclear density varies along the periodic table roughly in the range 0.14–0.22 fm^{-3}, the BRs shown in the figure do not change much over this range of densities. Therefore, the precise dependence on ρ may be neglected, and we assume that the $K^-N \to \pi\Lambda$ capture reaction takes place at a proton (or neutron) density $\rho = \rho_0/2$. For further applications, we denote the BRs obtained at nuclear density $\rho = \rho_0/2$ by BR1, and we denote the BRs obtained in vacuum by BR2.

The use of a microscopic model for the $K^-N \to \pi\Lambda$ BRs is one of the novelties of the present paper. Past works used BRs derived indirectly by extrapolating from measurements performed in carbon and freon emulsions [19], a procedure that is prone to systematic errors. We use these emulsion BRs (labeled here as BR3) to compare with BRs obtained from our microscopic chiral model. This is shown in Table I, where the maximum difference between the various BRs (BR1, BR2, and BR3) is as large as 30%. However, this variation is still small compared to other effects discussed as follows. The ratio of 1/2 for BRs on a proton to BRs on a neutron follows from charge independence, which is implemented by conserving isospin in our model for $K^-N \to \pi\Lambda$.

B. wave functions

To perform the numerical calculation of the DWIA integrals $I^{\ell}_{n_Y l_Y, n_N l_N}$ Eq. (13) and $\bar{\rho}_N$ Eq. (8), w.fs. of the initial kaon and nucleon and of the final hyperon and outgoing pion are needed. These w.fs. are generated by solving the respective wave equations with fitted potentials.

1. K^- wave functions

For the kaon w.f., we use the Klein-Gordon equation with a potential, which consists of two parts, the finite-size Coulomb potential plus first-order vacuum polarization corrections, and the strong-interaction optical potential parametrized phenomenologically by the form [20]:

$$V^K_{\rm opt}(r) = -\frac{4\pi}{2\mu_K}\left(1+\frac{\mu_K}{M_N}\right)\left\{b + B\left[\frac{\rho(r)}{\rho(0)}\right]^{\nu}\right\}\rho(r). \tag{14}$$

Here, μ_K stands for the kaon-nucleus reduced mass, M_N is the nucleon mass, and $\rho(r)$ denotes the nuclear density normalized to the number of nucleons A. We use three different parameter sets for the kaon-nucleus optical potential, as specified in Table II. In the last column of the table, for orientation, we show the approximate depth of the strong-interaction (real part) potentials at nuclear density $\rho = \rho_0 = 0.17$ fm^{-3}.

The meson-nuclear optical potential is often expressed by an effective scattering length multiplied by the nuclear density. Thus, the parameter b for the potential $[K_\chi]$ represents the average of the K^-n and K^-p scattering lengths in the nuclear medium computed by using the chiral model discussed in Sec. III A. The values of parameter sets for potentials $[K_{\rm eff}]$ and $[K_{\rm DD}]$ were fitted to reproduce a large set of kaonic atom data by Friedman *et al.* [20]. For $B = 0$, the potential reduces to the standard effective $[K_{\rm eff}]$ parametrization of the optical potential. The potential $[K_{\rm DD}]$ explicitly exhibits a substantial density dependence, which may be related to the dynamics of the $\Lambda(1405)$ resonance submerged into the nuclear medium [20].

For the targets considered in the present paper, the relevant K^--atomic orbits are represented by the $2P$ ($L = 1$) and $3D$ ($L = 2$) states. These are the lowest L orbits observed in the X-ray cascade and are sufficiently close to the nucleus for capture to occur significantly. The calculations were performed separately for each of these orbits, and a weighted average was then taken according to Batty's analysis of the atomic cascade process [21]. The relative populations of these $L = 1, 2$ atomic orbits (summed over n) are listed in Table III.

2. Baryon wave functions

The w.fs. of nucleons and hyperons were computed numerically as bound states in a Woods-Saxon potential,

$$V(r) = -\frac{V_0}{1+\exp\,(r-R)/a}, \qquad R = r_0 A^{1/3}, \tag{15}$$

with geometry fixed by setting $a = 0.6$ fm and $r_0 = 1.25$ fm. The potential depth V_0 was adjusted separately for each baryon

TABLE II. Parameters of the K^- nuclear optical potential Eq. (14).

Potential	b (fm)	B (fm)	ν	Re $V^K_{\rm opt}(\rho = \rho_0)$ (MeV)
$[K_\chi]$	$0.38 + 0.48i$	0	0	−50
$[K_{\rm eff}]$	$0.63 + 0.89i$	0	0	−80
$[K_{\rm DD}]$	$-0.15 + 0.62i$	$1.65 - 0.06i$	0.23	−190

TABLE III. Relative population of K^--atomic orbits [21].

Orbit	^{7}Li	^{9}Be	^{12,13}C	^{16}O
P	0.76	0.49	0.23	0.18
D	0.24	0.51	0.77	0.82

state so that the corresponding binding energy was reproduced; see Ref. [22] for a compilation of Λ hypernuclear binding energies.

3. Pion distorted waves

The pionic optical potential is taken to be of the standard form [23], often used in the analysis of pionic atoms and pion-nuclear scattering:

$$
\begin{aligned}
-\frac{2\mu_\pi}{4\pi}V^{\pi}_{\rm opt} &= \left(1+\frac{m_\pi}{M_N}\right)b_0\rho(r)+\left(1+\frac{m_\pi}{2M_N}\right)B_0\rho^2(r)\\
&\quad -\nabla\frac{\alpha(r)}{1+\frac{4\pi}{3}\xi\alpha(r)}\nabla,\\
\alpha(r) &= \left(1+\frac{m_\pi}{M_N}\right)^{-1}c_0\rho(r)\\
&\quad +\left(1+\frac{m_\pi}{2M_N}\right)^{-1}C_0\rho^2(r).
\end{aligned}
\tag{16}
$$

Here, μ_π stands for the pion-nuclear reduced mass, m_π and M_N are the pion and nucleon masses, and $\rho(r)$ denotes the nuclear density normalized to the number of nucleons A. Calculations were performed with a free (plane-wave) pion and with two different parameter sets for the pion-nuclear optical potential. These potentials were fitted to low-energy scattering data [24,25], and their parameters are listed in Table IV.

IV. RESULTS AND DISCUSSION

Here, we present the results of calculations of K^- capture rates for Λ hypernuclear production on p-shell targets and discuss their sensitivity to various inputs. It was assumed in these calculations that capture to the low-lying Λ hypernuclear bound states, or resonances, occurs only through baryon transitions $1p_N \to 1s_\Lambda$ and $1p_N \to 1p_\Lambda$ from the $1p_N$ valent shell to the $1s_\Lambda$ and $1p_\Lambda$ single-particle (s.p.) states, respectively, in the final hypernucleus. Since the experimental data on light hypernuclei often do not indicate distinct hypernuclear s.p. structure for the $1p_\Lambda$ configuration, we considered the production of $1p_\Lambda$ states only beginning with $A = 12$. Furthermore, we note that the multipolarity k in Eqs. (11) and (12) is limited to $k = 1$ (1^- transition) for the $1p_N \to 1s_\Lambda$ capture process, whereas two values $k = 0, 2$ are allowed in the $1p_N \to 1p_\Lambda$ capture process ($0^+, 2^+$ transitions). The number of valence nucleons $\mathcal{N}(1p_N)$, which contribute to the capture rates Eq. (11) is 2, 3, 4, 5, and 6 (neutrons) in the $(K^-_{\rm stop}, \pi^-)$ reaction for target nuclei ^{7}Li, ^{9}Be, ^{12}C, ^{13}C, and ^{16}O, respectively.

A. Sensitivity tests

1. Baryon wave functions

To test the sensitivity of our results to the baryon w.fs. generated by Woods-Saxon potentials Eq. (15), we calculated the capture rates for the production of $^{12}_{\Lambda}$C (in both the $1s_\Lambda$ and $1p_\Lambda$ states) for a modified geometry of the Woods-Saxon potential. Specifically, we used $A = 11, 13$ instead of $A = 12$ in Eq. (15). The difference in capture rates was less than 10%. We also varied the depth of the Woods-Saxon potential and checked that its variation by about 10% leads to a less than 5% difference in the capture rates. In general, realistic variations of the baryon w.fs. have a relatively small impact (less than 10%) on the calculated capture rates.

A further sensitivity test is demonstrated here for the ^{16}O target. Table V lists capture rates per hyperon, Eq. (11) per one p-shell neutron [$\mathcal{N}(n_N l_N) = 1$], obtained for a neutron in each one of the nuclear $1p_j$ subshells (with binding energies, which differ roughly by 6 MeV), for a $1s_\Lambda$ hyperon with binding energy given by the Λ separation energy in the hypernuclear ground state and for each one of the $2P$ and $3D$ K^- orbits. Except for the case of $2P$ and $[K_\chi]$, switching from $1p_{1/2}$ to $1p_{3/2}$ makes little difference, in agreement with the assumption that the relevant entities depend only weakly on the total angular momenta $j_B = l_B \pm 1/2$. However, the $2P$ orbit contribution is considerably weaker than that of the $3D$ orbit contribution in ^{16}O (see also Table III). Hence, this j dependence is negligible for the K^- $[K_\chi]$ potential, whereas it amounts to approximately a 10% effect for the K^- $[K_{\rm DD}]$ potential.

2. K^- capture branching ratios and wave functions

We start by discussing the sensitivity of the calculated capture rates to the choice of BRs for the $K^-N \to \pi\Lambda$ capture process. In Fig. 2, we show the capture rate per stopped kaon Eq. (6) calculated for the production of $^{12}_{\Lambda}$C in the $1s_\Lambda$ state for the K^--nucleus potential $[K_{\rm eff}]$ and the pion-nucleus potential π_c. We recall that BR1 and BR2 come from our chiral microscopic model, whereas BR3 is derived from emulsion experiments. It is seen that all the calculated rates are quite close to each other but are significantly lower than the experimental data [2]. Since the difference between capture rates, which corresponds to various $K^-N \to \pi\Lambda$ BRs

TABLE IV. Parameters of the pionic optical potential Eq. (17).

Potential	$b_0\,[m_\pi^{-1}]$	$B_0\,[m_\pi^{-4}]$	$c_0\,[m_\pi^{-3}]$	$C_0\,[m_\pi^{-6}]$	ξ
π_b	$0.268+0i$	0	$0.036+0.206i$	$0-0.203i$	1.4
π_c	$0.010+0.437i$	0	$0.047+0.222i$	0	0

TABLE V. Capture rates per hyperon and per one p-shell neutron (in units of 10^{-4}) calculated for different j orbits assumed for 1p-shell neutrons in ^{16}O, see text.

K^- orbit	$[K_\chi]$		$[K_{\rm DD}]$	
	$(1p_{1/2})_n$	$(1p_{3/2})_n$	$(1p_{1/2})_n$	$(1p_{3/2})_n$
$2P$	1.23	1.43	0.33	0.37
$3D$	2.64	2.67	0.66	0.72

is relatively small (30% at most) compared to uncertainties caused by other effects (K^--nucleus or π-nucleus potential), in this paper, we present results based exclusively on BR1 values, which correspond to a well-controlled in-medium chiral calculation.

The sensitivity to the K^- w.fs. for a given pion-nucleus potential (π_b) is demonstrated in Fig. 3, which shows calculated capture rates for the $1s_\Lambda$ state of $^{12}_{\Lambda}$B. with respect to the measured rate [3] (figures for other targets look similar). The calculated rates are presented in order of increasing depth of the K^--nucleus optical potential used to generate the kaon w.f., from a purely electromagnetic potential (zero depth) to the density-dependent potential $[K_{\rm DD}]$ (−190-MeV depth). The calculated capture rate appears to be a decreasing function of the K^--nucleus potential depth.

3. *Pion distorted waves*

Figure 4 shows the dependence of the capture rate on the choice of the pion-nucleus potential for the formation of $^{16}_{\Lambda}$O in the $1s_\Lambda$ configuration, which consists of two separate peaks roughly of structure $(np^{-1}_{1/2}\Lambda s_{1/2})$ and $(np^{-1}_{3/2}\Lambda s_{1/2})$ for the 1^- ground state and the 6-MeV first excited 1^- state [2]. One notes that pion distortion plays an important role. The difference between the results obtained with and without pion distortion is enormous. On the other hand, both pion optical potentials considered here lead to quite similar capture rates. The resulting rate for potential π_c is just a little smaller than the result for potential π_b, with values 0.154×10^{-3} (π_c) and 0.219×10^{-3} (π_b), to be compared with a measured summed $1s_\Lambda$ capture rate of 0.43 ± 0.06 [2].

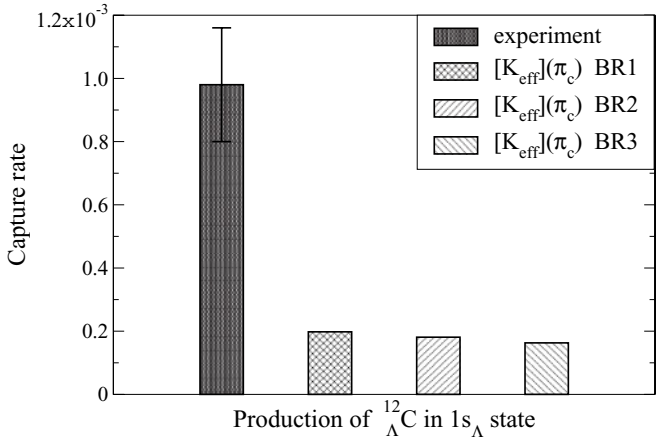

FIG. 2. Sensitivity of calculated $1s_\Lambda$ capture rates per stopped K^- in ^{12}C → $^{12}_{\Lambda}$C to $K^-n \to \pi^-\Lambda$ BRs, with respect to the measured summed $1s_\Lambda$ capture rate [2].

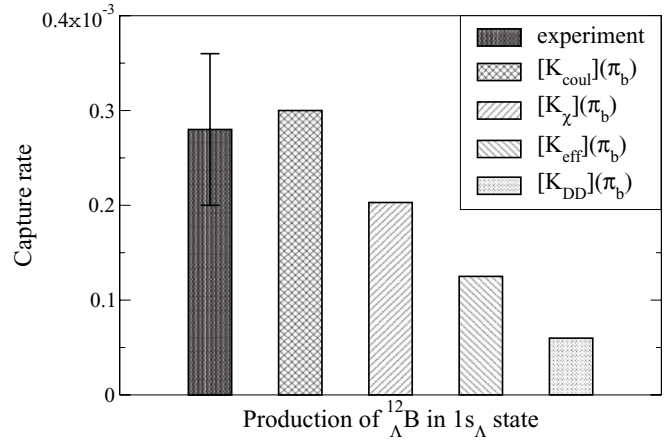

FIG. 3. Sensitivity of calculated $1s_\Lambda$ capture rates per stopped K^- in ^{12}C → $^{12}_{\Lambda}$B to K^- w.fs., with respect to the measured summed $1s_\Lambda$ capture rate [3].

B. Selected results

1. $1s_\Lambda$ *capture rates*

The capture rates calculated for the summed production of $1s_\Lambda$ states in $(K^-_{\rm stop}, \pi^-)$ reactions throughout the nuclear p shell are assembled in Table VI. We only show results obtained with pion-nucleus potential π_b and with kaon-nucleus potentials $[K_\chi]$ and $[K_{\rm DD}]$, which represent the two main directions for how the K^--nucleus interaction is treated at present. It appears that the $1s_\Lambda$ capture rate is a decreasing function of A throughout the nuclear p shell, with a rate of decrease which depends sensitively on the depth of the K^--nucleus potential. The ratio of $1s_\Lambda$ capture rate in ^{16}O to that in ^{7}Li is 2.66 for $[K_\chi]$ and 5.27 for $[K_{\rm DD}]$. Put differently, the ratio of rates related to the K^- relatively shallow chiral

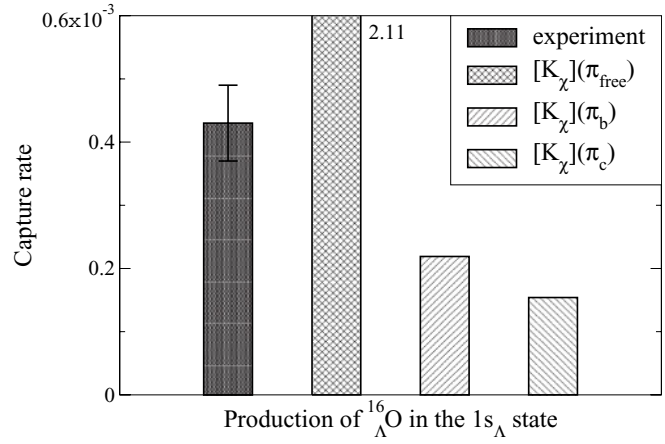

FIG. 4. Sensitivity of calculated $1s_\Lambda$ capture rates per stopped K^- in ^{16}O → $^{16}_{\Lambda}$O to pion DWs, with respect to the measured summed $1s_\Lambda$ capture rate [2].

TABLE VI. Calculated capture rates (in units of 10^{-3}) for the summed $1s_\Lambda$ production (1^- transitions) in p-shell nuclei, by using two variants for the K^--atomic w.fs.

K^- potential	${}^{7}_{\Lambda}$Li	${}^{9}_{\Lambda}$Be	${}^{12}_{\Lambda}$C	${}^{13}_{\Lambda}$C	${}^{16}_{\Lambda}$O
$[K_\chi]$	0.583	0.464	0.425	0.268	0.219
$[K_{\rm DD}]$	0.290	0.245	0.125	0.066	0.055

TABLE VIII. Variation of $\bar{\rho}_N$ Eq. (8) for $L = 2$ (in units of 10^{-10}) upon varying the ^{12}C and ^{13}C input.

K^-(C)	$[K_\chi]$		$[K_{\rm DD}]$	
	$\rho_N(^{12}\mathrm{C})$	$\rho_N(^{13}\mathrm{C})$	$\rho_N(^{12}\mathrm{C})$	$\rho_N(^{13}\mathrm{C})$
$K^-(^{12}\mathrm{C})$	2.47	2.88	3.41	3.98
$K^-(^{13}\mathrm{C})$	2.55	2.97	2.80	3.27

potential to rates related to the K^- relatively deep $[K_{\rm DD}]$ potential increases throughout the p shell, from approximately 2 for lithium up to about 4 for oxygen. This trend is caused by the node structure of the atomic w.fs. used in the DWIA amplitudes Eq. (13). Whereas in ^{7}Li, the atomic $3D$ w.fs. are nodeless within the nucleus, and the suppression of the rate for $[K_{\rm DD}]$ with respect to $[K_\chi]$ is caused by a node in (the real part of) the $[K_{\rm DD}]$ $2P$ w.f., in ^{16}O the $[K_{\rm DD}]$ $3D$ w.f. too has a node within the nucleus, which leads to further suppression with respect to the rate calculated for the $[K_\chi]$ nodeless $3D$ w.f. Nodes of atomic w.fs. within the nucleus are linked to the existence of quasibound K^--nuclear states [26]. The deeper $[K_{\rm DD}]$ potential generates such $L = 1$ quasibound nuclear states throughout the p shell and $L = 2$ states beginning with the carbon isotopes, whereas the shallower $[K_\chi]$ potential has $L = 1$ states which only begin with the carbon isotopes and no $L = 2$ quasibound nuclear states throughout the p shell.

We note the relatively sizable drop of the calculated $1s_\Lambda$ capture rates in going from ^{12}C to ^{13}C. To identify its origin, we analyzed the impact of each one of the w.fs., which appear in the DWIA amplitude Eq. (13) in the carbon region (except for the remarkably stable $1s_\Lambda$ w.f.) on the most important $|I^{\ell}_{1s,1p}|^2$ contribution. This procedure is demonstrated in Table VII where by starting with ^{12}C related K^-, π^-, and neutron w.fs. in the first row, we successively replaced them by ^{13}C related w.fs. as specified in the first column of rows 2–4. The replacement of the K^- w.f., in particular, is seen to have a small effect for the $[K_\chi]$ chiral potential w.f., but a large effect for the $[K_{\rm DD}]$ w.f. The successive replacement of other w.fs., particularly the oscillating pion DW, leads to further suppression for both $[K_\chi]$ and $[K_{\rm DD}]$.

In Table VIII, we show the variation of the effective nuclear density Eq. (8), which appears in the denominator of Eq. (11) for the capture rate. The resultant effect is considerably more moderate than for the $[K_{\rm DD}]$ DWIA amplitude listed in Table VII, simply because the two components of the $\bar{\rho}_N$ integrand are each positive definite and are less sensitive to the position of nodes in the $[K_{\rm DD}]$ $3D$ atomic w.f. The net outcome of the variations studied in Tables VII and VIII is a considerably smaller capture rate for ^{13}C than for ^{12}C, at least for $[K_{\rm DD}]$. For $[K_\chi]$, the reduction appears weaker (it is more effective in some of the other $|I^{\ell}_{1s,1p}|^2$ contributions not shown here).

TABLE VII. Variation of the most dominant $|I^{\ell}_{1s,1p}|^2$ contribution Eq. (13) for $L = 2$ and pion DWs ($\pi_{\rm b}$) (in units of 10^{-12}) upon going from ^{12}C to ^{13}C.

Path of variation	$\lvert I^{3}_{1s,1p}\rvert^2([K_\chi])$	$\lvert I^{1}_{1s,1p}\rvert^2([K_{\rm DD}])$
^{12}C	3.92	1.44
+ Kaon w.f.	3.90	0.74
+ Pion w.f.	2.77	0.51
+ Neutron w.f. = ^{13}C	2.70	0.42

2. $1p_\Lambda$ capture rates

Calculated capture rates for the $1p_N \to 1p_\Lambda$ 0^+ and 2^+ transitions [see Eq. (11)] are presented in Table IX for ^{12}C and ^{16}O targets. For completeness, we also included the $1p_N \to 1s_\Lambda$ 1^- transition discussed in Sec. IV B 1 and added experimental rates from KEK [2] and BNL [3]. Here, the reason for choosing KEK over CERN [1] and FINUDA [4] is that for ${}^{12}_{\Lambda}$C production, the KEK [2] rates are the closest to the isospin factor 2 expected in getting these rates from the ${}^{12}_{\Lambda}$B rates, which were measured only at BNL [3].[2] Of course, if further $(K^-_{\rm stop}, \pi^0)$ experiments are done on ^{12}C, which would lead to different results from those of Ref. [3], one's preference might change accordingly.[3] Similar to the summed $1s_\Lambda$ rate discussed in Sec. IV B 1 the summed $1p_\Lambda$ rate for the deep potential $[K_{\rm DD}]$ is smaller by a factor of 3 to 4 than for the relatively shallow potential $[K_\chi]$. By excluding the old CERN data [1], the calculated $1p_\Lambda$ capture rates are generally smaller than the experimentally reported rates, with the exception that the $[K_\chi]$ rates for ${}^{12}_{\Lambda}$B are larger than the reported rate [3]. Since the $1p_\Lambda$ spectral strength is partly mixed into the $(K^-_{\rm stop}, \pi)$ quasifree continuum, and its extraction from the measured spectra is considerably more ambiguous than the extraction of the summed $1s_\Lambda$ production rate, we do not proceed further to confront theory with experiment for the summed $1p_\Lambda$ production rate.

V. CONCLUSION

We performed DWIA $(K^-_{\rm stop},\pi)$ calculations for p-shell targets, using several K^- and pion w.fs. to test the sensitivity of the calculated hypernuclear capture rates on the choice of these w.fs. The calculated capture rates are generally smaller than

[2]The reported summed $1s_\Lambda$ capture rate in ${}^{12}_{\Lambda}$C varies from $(0.2 \pm 0.1) \times 10^{-3}/K^-$ [1] to $(1.86 \pm 0.14) \times 10^{-3}/K^-$ [4].

[3]The ratio of the calculated $1s_\Lambda$ capture rate to ${}^{12}_{\Lambda}$C over that of ${}^{12}_{\Lambda}$B is largely caused by the ratio of the $K^-N \to \pi\Lambda$ BRs, which, in the limit of good isospin, is 2. A slight departure from this ratio is caused by charge-dependent effects in our calculation, notably from the outgoing pion DWs.

TABLE IX. Calculated capture rates per stopped K^- (in units of 10^{-3}) for production of $1s_\Lambda$ states (1^- transition) and $1p_\Lambda$ states (0^+ and 2^+ transitions) and selected experimental rates.

Transition	Input	${}^{12}_{\Lambda}$B [3]	${}^{12}_{\Lambda}$C [2]	${}^{16}_{\Lambda}$O [2]
1^-	$[K_\chi]$	0.203	0.425	0.219
	$[K_{\rm DD}]$	0.060	0.125	0.055
	Experimental rates	0.28 ± 0.08	0.98 ± 0.12	0.43 ± 0.06
0^+	$[K_\chi]$	0.096	0.216	0.134
	$[K_{\rm DD}]$	0.011	0.021	0.020
2^+	$[K_\chi]$	0.547	1.052	0.872
	$[K_{\rm DD}]$	0.192	0.410	0.330
$0^+ + 2^+$	$[K_\chi]$	0.643	1.268	1.006
	$[K_{\rm DD}]$	0.203	0.431	0.350
	Experimental rates	0.35 ± 0.09	2.3 ± 0.3	1.68 ± 0.16

the measured ones; the deeper the K^- potential, the smaller is the capture rate. Since the absolute normalization of capture at rest experimental rates is a delicate matter, we suggest to focus on the A dependence of the measured rates, expecting it to be largely free of the absolute normalization of the data. The calculated capture rates for a given K^- optical potential decrease as a function of A, with the fractional difference between the rates calculated for the two extreme K^- optical potentials, the shallow $[K_\chi]$ and the deep $[K_{\rm DD}]$, increasing steadily with A. We find other dependencies of the calculated capture rates to be secondary to the dependence on the K^--atomic w.f. in the range studied here. We argue that a dedicated experimental study of $1s_\Lambda$ capture rates in p-shell targets, such as reported recently by the FINUDA Collaboration in a preliminary form [6], could yield useful information on the depth of the threshold K^- optical potential by comparing the measured A dependence with the A dependence of the calculated capture rates listed in Table VI.

ACKNOWLEDGMENTS

This work was supported by the GAUK Grant No. 91509 and the GACR Grant No. 202/09/1441, as well as by the EU initiative FP7, HadronPhysics2, under Project No. 227431.

[1] M. A. Faessler *et al.*, Phys. Lett. B **46**, 468 (1973).
[2] H. Tamura, R. S. Hayano, H. Outa, and T. Yamazaki, Prog. Theor. Phys. Suppl. **117**, 1 (1994).
[3] M. W. Ahmed *et al.*, Phys. Rev. C **68**, 064004 (2003).
[4] M. Agnello *et al.*, Phys. Lett. B **622**, 35 (2005).
[5] M. Agnello *et al.*, in *Hypernuclear and Strange Particle Physics HYP2006*, edited by J. Pochodzalla and Th. Walcher (SIF and Springer, Berlin/Heidelberg, 2007) p. 57.
[6] M. Agnello *et al.*, Nucl. Phys. A **835**, 414 (2010) [presented by G. Bonomi for the FINUDA Collaboration at HYP-X, Tokai, Sept. 2009].
[7] J. Hüfner, S. Y. Lee, and H. A. Weidenmüller, Nucl. Phys. A **234**, 429 (1974).
[8] A. Gal and L. Klieb, Phys. Rev. C **34**, 956 (1986).
[9] A. Matsuyama and K. Yazaki, Nucl. Phys. A **477**, 673 (1988).
[10] A. Cieplý, E. Friedman, A. Gal, and J. Mareš, Nucl. Phys. A **696**, 173 (2001).
[11] V. Krejčiřík and A. Cieplý, Acta Phys. Pol. B **41**, 317 (2010).
[12] N. Kaiser, P. B. Siegel, and W. Weise, Nucl. Phys. A **594**, 325 (1995).
[13] T. Waas, N. Kaiser, and W. Weise, Phys. Lett. B **365**, 12 (1996).
[14] E. Oset and A. Ramos, Nucl. Phys. A **635**, 99 (1998).
[15] B. Borasoy, R. Nissler, and W. Weise, Eur. Phys. J. A **25**, 79 (2005).
[16] A. Cieplý and J. Smejkal, Eur. Phys. J. A **34**, 237 (2007).
[17] A. Cieplý and J. Smejkal, Eur. Phys. J. A **43**, 191 (2010).
[18] M. Lutz, Phys. Lett. B **426**, 12 (1998).
[19] C. Vander Velde-Wilquet *et al.*, Nuovo Cimento A **39**, 538 (1977).
[20] E. Friedman, A. Gal, and C. J. Batty, Nucl. Phys. A **579**, 518 (1994).
[21] C. J. Batty (private communication, 1995).
[22] O. Hashimoto and H. Tamura, Prog. Part. Nucl. Phys. **57**, 564 (2006).
[23] M. Ericson and T. E. O. Ericson, Ann. Phys. **36**, 323 (1966).
[24] H. A. Thiessen *et al.*, LAMPF Report No. LA-7607-PR, 1978 (unpublished).
[25] C. J. Harvey *et al.*, LAMPF Report No. LA-UR-84-1732, 1984 (unpublished).
[26] C. J. Batty, E. Friedman, and A. Gal, Phys. Rep. **287**, 385 (1997).